

Observation of multiple pairing modes in the 2D Hubbard Model

Rayan Farid, Maxence Grandadam, and J. P. F. LeBlanc*

*Department of Physics and Physical Oceanography, Memorial University of Newfoundland,
St. John's, Newfoundland & Labrador, Canada A1B 3X7*

(Dated: January 20, 2023)

We compute the diagrammatic expansion of the particle-particle susceptibility via algorithmic Matsubara integration and compute the correlated pairing susceptibility in the 2D Hubbard Model. We study the static susceptibility and its dependence on the pair momentum \mathbf{q} for a range of temperature, interaction strength and chemical potential. We show that $d_{x^2-y^2}$ -wave pairing is expected in the model in the $U/t \rightarrow 0^+$ limit from direct perturbation theory. From this, we identify key second and third-order diagrams that support pairing processes. We find two key components for pairing at momenta $(0,0)$ and (π,π) that can be well fit as separate bosonic modes. We extract amplitudes and correlation length scales where we find a predominantly local (π,π) pairing and non-local $\mathbf{q} = (0,0)$ pairs and present the relative weights of these modes for variation in temperature, doping, and interaction strength.

Introduction: Understanding the mechanisms by which electronic correlations drive phase transitions remains a dominant motivation for the development of numerical approaches for solving correlated electron systems. The two-dimensional Hubbard model has been heavily studied in this respect[1, 2] and is thought to be the quintessential representation of high transition temperature cuprate materials since the model, despite its simplicity, contains metallic, insulating, pseudogap and superconducting phases when studied by non-perturbative approaches on finite-sized systems.[3–6] There the finite-size approach allows for a second-order phase transition to the superconducting state while a truly infinite system cannot due to the Mermin Wagner theorem. Nevertheless, perturbative expansions at high order on infinite systems find corroborating physics in the model; metallic, insulating, and pseudogap features in single-particle properties without the need for infinite range correlations.[2, 7] In all cases, the dominant excitations leading to insulating and pseudogap behaviour are antiferromagnetic $\mathbf{q} = (\pi,\pi)$ spin excitations and this has been shown explicitly via fluctuation diagnostics methods[8–10] and rigorously tested by a variety of numerical approaches.[2] To complicate matters, recent works[11, 12] have shown that the dominant excitation responsible for an anomalous self-energy is identical to the dominant excitation thought to lead to insulating behaviour, primarily static (π,π) spin-excitations.

For the general problem, particle pairing is governed by a Bethe-Salpeter equation for the particle-particle susceptibility $\chi^{pp} = \chi_0 + \chi_0 F \chi_0$ where χ_0 is given by the dressed particle-particle bubble and all pair-correlations are described by the insertion of the full vertex F . Correlated pairing processes are therefore a property of only vertex diagrams, and in the case of the Hubbard model, these have been somewhat studied via non-perturbative approaches by computing the correlated pairing susceptibility $P_g(\mathbf{q}, \Omega) = \chi_{pp}^g(\mathbf{q}, \Omega) - \chi_0^g(\mathbf{q}, \Omega)$ that is nothing more than the vertex contributions projected into the

$g = s, p, d...$ channels.[13–16] Existing studies of the pairing susceptibility are from non-perturbative approaches such as the dynamical cluster approximation that have very limited momentum space resolution.[6, 17] From perturbative expansions very little is known since the simplest vertex terms, the RPA-like ladder series does not give rise to divergent behaviour when projected into the d -wave channel. The application of a form factor strongly suppresses the ladder diagrams when scattering momenta \mathbf{q} is along its nodal line rendering the ladder expansion ineffectual.

In this work, we directly compute the full perturbative expansion of the vertex contributions to the particle-particle susceptibility. This is possible due to algorithmic advances that provide partially analytic expressions to arbitrarily complex Feynman diagrams without finite size approximations.[18–23]. We study the full \mathbf{q} -dependence of the static pairing-susceptibility and impose a variety of symmetry factors to extract the susceptibility of the system to s -wave, p -wave, and d -wave symmetries. Our results are extraordinarily consistent with previous works, both perturbative and non-perturbative, and we identify the primary components of pairing.

Hubbard Hamiltonian: We study the single-band Hubbard Hamiltonian on a 2D square lattice[1],

$$H = \sum_{ij\sigma} t_{ij} c_{i\sigma}^\dagger c_{j\sigma} + U \sum_i n_{i\uparrow} n_{i\downarrow}, \quad (1)$$

where t_{ij} is the hopping amplitude, $c_{i\sigma}^{(\dagger)}$ ($c_{i\sigma}$) is the creation (annihilation) operator at site i , $\sigma \in \{\uparrow, \downarrow\}$ is the spin, U is the onsite Hubbard interaction, $n_{i\sigma} = c_{i\sigma}^\dagger c_{i\sigma}$ is the number operator. We restrict the sum over sites to nearest and next-nearest neighbors for a 2D square lattice, resulting in the free particle energy

$$\epsilon(\mathbf{k}) = -2t[\cos(k_x) + \cos(k_y)] - 4t'[\cos(k_x)\cos(k_y)] - \mu,$$

where μ is the chemical potential, and $t(t')$ is the nearest (next-nearest) neighbor hopping amplitude. Throughout, we work with energies in units of the hopping, $t = 1$,

and primarily study the $t' = 0$ case. Data for $t' \neq 0$ is provided in the supplemental materials.

Perturbative Expansion: The pairing process relevant to superconductivity is the pairing between a spin-up electron with momentum $\mathbf{k} + \mathbf{q}$ and a spin-down with momentum $-\mathbf{k}$. In the BCS limit, this is expected to be dominated by a zero momentum pair given for $|\mathbf{q}| = 0$. The particle-particle susceptibility projected into a particular symmetry is given by

$$\chi_{pp}^g(\mathbf{q}, \tau) = \langle \gamma_{\mathbf{k}+\mathbf{q}} c_{\mathbf{k}+\mathbf{q}\uparrow}(\tau) c_{-\mathbf{k}\downarrow}(\tau) c_{-\mathbf{k}\downarrow}^\dagger(0) c_{\mathbf{k}'+\mathbf{q}\uparrow}^\dagger(0) \gamma_{\mathbf{k}'+\mathbf{q}} \rangle. \quad (2)$$

We evaluate this expectation value via a perturbative expansion for the Hubbard interaction, and this gives rise to a set of Feynman diagrams, a subset of which are depicted in Fig. 1. These are the set of all vertex diagrams that contribute to the correlated pairing susceptibility $P_g(\mathbf{q}, \Omega)$. [15, 24, 25] This susceptibility is a function of the momentum difference \mathbf{q} and frequency Ω of the external bosonic line. Throughout we will study the static quantity $P_g(\mathbf{q}) = P_g(\mathbf{q}, \Omega = 0)$. The subscript g represents the choice of s, p, d -wave projection and determines the functions $\gamma_{\mathbf{k}+\mathbf{q}}$ and $\gamma_{\mathbf{k}'+\mathbf{q}}$ that represent initial and final momenta along a single particle line. We convert each Feynman diagram to an analytic expression that is treated symbolically via algorithmic Matsubara integration (AMI) [18–20] which performs Matsubara summation analytically. This represents fully one-third of the internal integrations being exact to machine precision with virtually zero computational expense. The remaining spatial integrals are performed using integration methods for continuous functions. The functions to be integrated are too complex to write by hand as the Matsubara sums generate a large number of analytic terms. Further details on AMI are provided in the supplemental.

We proceed in an order-by-order perturbative expansion in powers of U/t starting from small U/t values. This has of course the disadvantage that there is a factorial growth in the diagram space for increasing order, as well as the expansion necessitates studying the weak-coupling limit where U/t is relatively small. The advantage to this approach is that there is no finite-size approximation, the results are already in the thermodynamic limit, and because of this, there will always exist a region of the phase diagram (small U/t , high temperature, heavily doped) where the perturbative expansion remains controlled and results are virtually exact.

We present this expansion up to fifth order in Fig. 2 for the half-filled case at $\mathbf{q} = (0, 0)$, $\beta t = 5$, and $U/t = 3$ for s - and $d_{x^2-y^2}$ -wave symmetries. We stress that in 5th order the results represent the sum of 544 diagrams that together are comprised of 559812 analytic terms to be integrated. We contrast the contributions from all diagrams to contributions from only ladder diagrams - those accessible analytically by hand. In the case of s -wave, Fig. 2(a), the dominant first-order ladder diagram is neg-

ative and opposes pairing. The contributions then alternate sign order-by-order, but the negative value of the first order diagram makes s -wave pairing impossible in the $U/t \rightarrow 0^+$ limit. Conversely, in the attractive interaction $U < 0$ regime, the pairing is predominately an s -wave $\mathbf{q} = (0, 0)$ process driven by ladder diagrams. We see also that the non-ladder diagrams act to suppress the ladder diagrams at each order but do not change the qualitative behavior. The $d_{x^2-y^2}$ -wave case in Fig. 2(b) is entirely different. Here the $\gamma_{\mathbf{k}}$ projection factors become independent of each other for ladder diagrams in the $|\mathbf{q}| \rightarrow 0$ limit and produce zero contribution to pairing at every order. Hence, the ladder diagrams neither promote nor *oppose* $d_{x^2-y^2}$ -wave pair formation, and this results in a dominant and positive second-order pairing susceptibility. This provides the potential for pairing even in the $U/t \rightarrow 0$ limit. Here shown for the half-filled problem, we find also positive contributions for the third order followed by competition at fourth order and a small negative 5th-order contribution. The sequence of positive second and third-order terms gives rise to a substantial range of U/t where positive contributions exist before being squashed by higher-order terms. Additional details and calculations on the order-by-order breakdown and pairing in p and d_{xy} -wave channel are provided in the supplemental.

Momentum and Doping Dependence: In order to focus on the dominant positive contributions to the $d_{x^2-y^2}$ pairing that appears at second and third order we truncate the expansion at third order which allows us to quickly sweep through density and the full momentum dependence which we depict in the top row of Fig. 3. The three panels are for high, intermediate, and low temperatures at $U/t = 3.0$ as a function of high symmetry cuts in scattering momentum \mathbf{q} and variation in chemical potential. At high temperatures, the susceptibility amplitude is weak, is centered near the half-filling point at $\mu = 0$, and appears most robust near the momentum vector $\mathbf{q} = (\pi, 0)$. As the temperature decreases we see that by $\beta t = 4$ much stronger features emerge at $\mathbf{q} = (0, 0)$ and surprisingly at $\mathbf{q} = (\pi, \pi)$. Decreasing temperature further the $\mathbf{q} = (\pi, \pi)$ peak is suppressed and the pairing is dominated by zero momentum pairing as expected. This evolution in pairing occurs over a range of temperatures where a variety of processes are known to take place in the 2D Hubbard model such as the presence of a pseudogap and also a metal-insulator crossover. [2, 7]

We emphasize the temperature dependence of the color-plot by presenting the $\mu = 0$ cuts in the lower row of Fig. 3. At high temperatures, the amplitude is extremely weak (on the scale of 10^{-3}) with a peak near $\mathbf{q} = (\pi, 0)$. As temperature decreases the dominant features are that of the second-order diagrams (see supplemental) that already shows two separate peaks at $\mathbf{q} = (0, 0)$ and (π, π) . Decreasing temperature further we see these peaks become sharper while the peak height at zero momentum

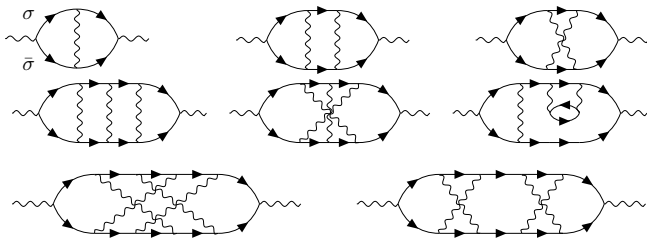


FIG. 1: A subset of Feynman diagrams responsible for the vertex correction to pairing. Straight lines with arrowhead and wavy lines correspond to single particle fermionic propagators and onsite interactions U/t respectively. The number of wavy lines determines the order. Onsite interaction must be between opposite spin as a consequence of Pauli's exclusion principle $\sigma \neq \bar{\sigma} \in \uparrow\downarrow$

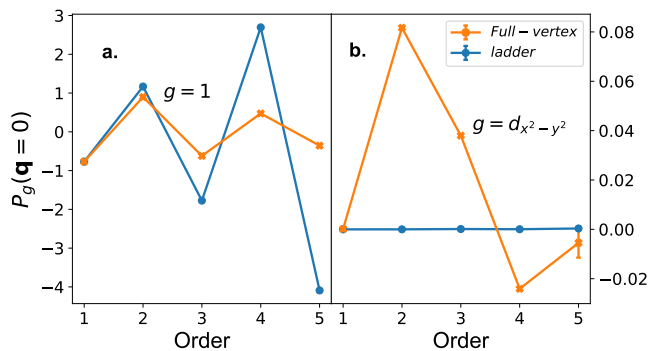


FIG. 2: Order-by-order contribution to static pairing susceptibility at half filling, $\beta t = 5$, and $U/t = 3.0$ for two symmetry factors: (a) P_S pairing for the full vertex contribution and its ladder constituents alternate signs with each order. (b) $P_{d_{x^2-y^2}}$ pairing is governed by non-ladder process with ladder diagrams making no contribution to the full vertex component. The second and third order promotes pairing while the fourth and fifth order represses it.

is dominant.

Fitting a two-component pairing: There exists a range of temperature and U/t values where the result of $P_{d_{x^2-y^2}}$ can be precisely fit by two Lorentzian functions, one centered at $\mathbf{q} = (0, 0)$ and a second at $\mathbf{q} = (\pi, \pi)$. We emphasize that this is not apparent in the analytics of the diagrammatic expansions that when truncated at third order include the sum of 730 analytic terms each integrated over a $2(n+1)$ dimensional space at order n . We define a fitting function as a sum of two Lorentzian $A(\mathbf{q}_0, \xi_0) + A(\mathbf{q}_p, \xi_p)$ where

$$A(\mathbf{q}_0, \xi_0) = \frac{W_0 \xi_0^{-1}}{q_x^2 + q_y^2 + \xi_0^{-2}} \quad (3)$$

$$A(\mathbf{q}_p, \xi_p) = \frac{W_p \xi_p^{-1}}{(q_x - \pi)^2 + (q_y - \pi)^2 + \xi_p^{-2}}.$$

By fitting along the diagonal \mathbf{q} direction we can extract two correlation length scales (ξ_0 and ξ_p) and two weights

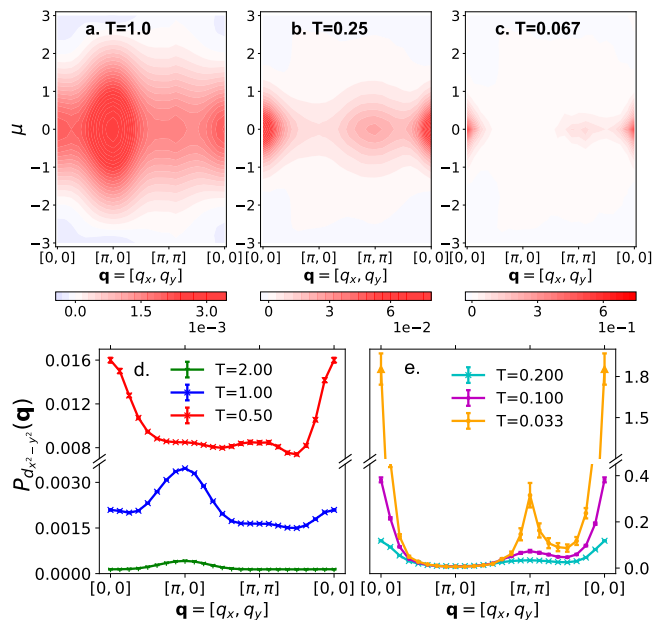


FIG. 3: (a-c) Contour plot for $d_{x^2-y^2}$ pairing across momentum symmetry cuts as a function of doping at $U/t = 3$ for (a) $T = 1.0t$, (b) $T = 0.25t$, (c) $T = 0.067t$. (d-e) the momentum evolution of pairing for various temperatures at $\mu = 0$ and $U/t = 3$

(W_0 and W_p) for $\mathbf{q} = (0, 0)$ and $\mathbf{q} = (\pi, \pi)$ respectively. An example fit is shown in Fig. 4 at $\beta t = 4$. We see that such a model of the data is an extremely good fit and this provides a picture of a very broad pairing mode at $\mathbf{q} = (\pi, \pi)$ and a sharper mode at $\mathbf{q} = (0, 0)$. We analyze the evolution of spectral weight and correlation lengths in Fig. 4(b-g). As a function of temperature, shown in Fig. 4(b-c) we find that ξ_p is rather flat and less than one lattice constant while the correlation length for the $\mathbf{q} = (0, 0)$ mode is greater than one for $\beta t > 3$ and is growing exponentially. The weight of each mode and their ratio are shown in the inset of Fig. 4(c). Both W_0 and W_p grow as the temperature is decreased while the ratio W_p/W_0 is roughly linear until $\beta t = 10$. For temperatures below this, the W_0 mode begins to dominate for this interaction strength of $U/t = 3$. This temperature scale coincides with a metal-insulator crossover known to occur here.[7] We see a continual growth of ξ_0 for reduced temperatures, shown in units of the lattice spacing we see that this pairing process remains short range on the scale of $1 \rightarrow 3$ lattice spacings. This is not the case for ξ_p that remains pinned at values less than one lattice spacing, indicating that this peak is a predominantly local pairing process. By fixing temperature $\beta t = 4$ we plot similar quantities as a function of chemical potential and again we see ξ_p is independent of μ while ξ_0 increases with doping while its amplitude decays. While a weak effect at this temperature, this leads to a range of μ where $\mathbf{q} = (0, 0)$ mode dominates $W_p/W_0 < 1$ and a region

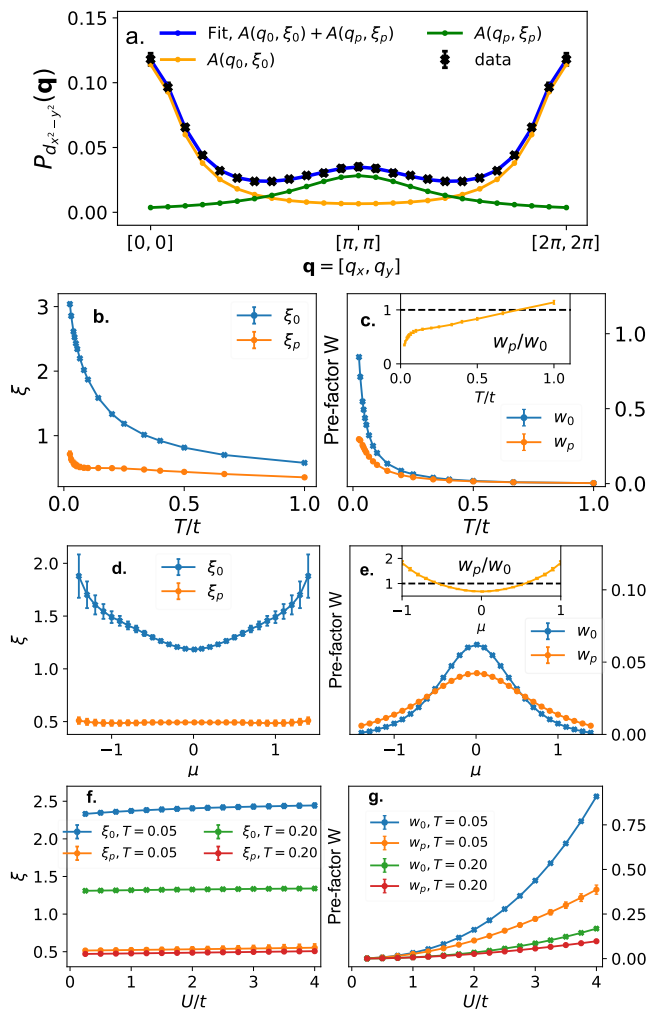


FIG. 4: (a) Example fitting via Eq. (3). (b-g) extracted correlation lengths (ξ_0 and ξ_p) in the units of lattice constant and weights (W_0 and W_p) (b,c) the temperature dependence at $\mu = 0$ and $U/t = 3$. (d,e) doping dependence at $T = 0.25$ and $U/t = 3$. (e,f) interaction strength U/t dependency at $\mu = 0$ for temperatures $T = 0.20t$ and $T = 0.05t$. Figure insets show the ratio between W_p and W_0

where $W_p/W_0 > 1$ and the $\mathbf{q} = (\pi, \pi)$ mode is dominant. Nevertheless, at half-filling, we see that the two modes have comparable weight. The doped $W_p/W_0 > 1$ region also roughly coincides where the competition with p - and d_{xy} -wave pairing is observed (see supplemental). Interestingly, neither ξ_0 nor ξ_p is strongly dependent upon the interaction strength, which we explore in Fig. 4(f-g). We see, however, that the weight of the modes scales dramatically with U/t values.

Role of t' : The inclusion of non-zero next-nearest neighbor hopping, t' , appears to have no qualitative effect on the results we present except for a shift of all peak features towards the hole-doped side of the phase diagram and overall weakening of $d_{x^2-y^2}$ pairing. Of note, we find

at least one case, when $t' = -0.3$, where it is possible to have only $\mathbf{q} = (\pi, \pi)$ pairing while the susceptibility to $\mathbf{q} = (0, 0)$ pairing remains negative. For completeness, we include results in the supplemental materials.

Discussion: By including a repulsive local Hubbard interaction we have found the existence of positive pairing due to vertex interactions in the weak coupling limit. We find two dominant momenta for which pairing occurs, the ‘standard’ zero momentum process that we find remains correlated over a short length scale, $\xi_0/a > 1$, and also an unexpected $\mathbf{q} = (\pi, \pi)$ pairing of a purely local nature, $\xi_0/a < 1$. These observations are robust at intermediate temperatures and exist already in the weak coupling regime at $U/t = 2$ that has been heavily studied recently.[2] We find that the integrated weight of these two components favours $\mathbf{q} = (0, 0)$ at low temperature and half-filling but that contributions from the (π, π) mode have a substantial contribution to local pairing and dominate at high temperature and away from half-filling. Further, we show explicitly that the dominant positive d -wave pairing comes from non-ladder diagrams, a single diagram at second order (with crossed interaction lines) as well as the sum of all 12 third order diagrams. We expect that for this model the higher order diagrams will suppress pairing for larger U/t values and low temperatures which will prevent an infinite range superconducting state except at $T = 0$ as required by the Mermin-Wagner theorem. Nevertheless, finite range pairing exists at accessible temperatures and we have shown estimates for the pairing length scales of each mode.

The physical picture that emerges is one of an interaction driven short ranged pairing between two electrons travelling with opposite momenta and spin $k \uparrow$ and $-k \downarrow$ (the $\mathbf{q} = (0, 0)$ case) but also rather large contributions from a local collective mode traveling in the (π, π) direction. One can visualize this process as the simultaneous hopping of pairs along the diagonal.

We can also speculate as to how our pairing processes relate to insulating and pseudogapped behavior observed in single-particle properties.[2, 7] The predominant theory is that bosonic $\mathbf{q} = (\pi, \pi)$ spin excitations couple with electron quasiparticles to form both the pseudogap and insulating behaviors that are observed in the 2D Hubbard model. From our results, we conclude that the insulating behavior may also coincide with non-local but finite range $\mathbf{q} = (0, 0)$ pair correlations. We would propose that the formation of pairs is not a competitive process with spin excitations but rather than $\mathbf{q} = (\pi, \pi)$ spin excitations act as the mediator of both $\mathbf{q} = (0, 0)$ and $\mathbf{q} = (\pi, \pi)$ pair correlations that might be responsible for opening a gap or pseudogap in the single-particle spectra as long suggested by mean-field RVB singlet models[26, 27].

We acknowledge the support of the Natural Sciences and Engineering Research Council of Canada (NSERC) RGPIN-2022-03882 and support from the Simons Collaboration on the Many Electron Problem.

-
- * jleblanc@mun.ca
- [1] J. P. F. LeBlanc, A. E. Antipov, F. Becca, I. W. Bulik, G. K.-L. Chan, C.-M. Chung, Y. Deng, M. Ferrero, T. M. Henderson, C. A. Jiménez-Hoyos, E. Kozik, X.-W. Liu, A. J. Millis, N. V. Prokof'ev, M. Qin, G. E. Scuseria, H. Shi, B. V. Svistunov, L. F. Tocchio, I. S. Tupitsyn, S. R. White, S. Zhang, B.-X. Zheng, Z. Zhu, and E. Gull (Simons Collaboration on the Many-Electron Problem), *Phys. Rev. X* **5**, 041041 (2015).
- [2] T. Schäfer, N. Wentzell, F. Šimkovic, Y.-Y. He, C. Hille, M. Klett, C. J. Eckhardt, B. Arzhang, V. Harkov, F. m. c.-M. Le Régent, A. Kirsch, Y. Wang, A. J. Kim, E. Kozik, E. A. Stepanov, A. Kauch, S. Andergassen, P. Hansmann, D. Rohe, Y. M. Vilk, J. P. F. LeBlanc, S. Zhang, A.-M. S. Tremblay, M. Ferrero, O. Parcollet, and A. Georges, *Phys. Rev. X* **11**, 011058 (2021).
- [3] H. Park, K. Haule, and G. Kotliar, *Phys. Rev. Lett.* **101**, 186403 (2008).
- [4] E. Gull and A. J. Millis, *Phys. Rev. B* **86**, 241106 (2012).
- [5] E. Gull, O. Parcollet, and A. J. Millis, *Phys. Rev. Lett.* **110**, 216405 (2013).
- [6] X. Chen, J. P. F. LeBlanc, and E. Gull, *Phys. Rev. Lett.* **115**, 116402 (2015).
- [7] F. Šimkovic, J. P. F. LeBlanc, A. J. Kim, Y. Deng, N. V. Prokof'ev, B. V. Svistunov, and E. Kozik, *Phys. Rev. Lett.* **124**, 017003 (2020).
- [8] O. Gunnarsson, T. Schäfer, J. P. F. LeBlanc, E. Gull, J. Merino, G. Sangiovanni, G. Rohringer, and A. Toschi, *Phys. Rev. Lett.* **114**, 236402 (2015).
- [9] B. Arzhang, A. E. Antipov, and J. P. F. LeBlanc, *Phys. Rev. B* **101**, 014430 (2020).
- [10] W. Wu, M. Ferrero, A. Georges, and E. Kozik, *Phys. Rev. B* **96**, 041105 (2017).
- [11] X. Dong, L. D. Re, A. Toschi, and E. Gull, Proceedings of the National Academy of Sciences **119**, e2205048119 (2022), <https://www.pnas.org/doi/pdf/10.1073/pnas.2205048119>.
- [12] X. Dong, E. Gull, and A. J. Millis, *Nature Physics* **10.1038/s41567-022-01710-z** (2022).
- [13] T. A. Maier and D. J. Scalapino, *npj Quantum Materials* **4**, 30 (2019).
- [14] M. Sigrist and K. Ueda, *Rev. Mod. Phys.* **63**, 239 (1991).
- [15] D. J. Scalapino, *Rev. Mod. Phys.* **84**, 1383 (2012).
- [16] C. C. Tsuei and J. R. Kirtley, *Rev. Mod. Phys.* **72**, 969 (2000).
- [17] D. Scalapino, in *Handbook of High-Temperature Superconductivity*, edited by J. Schrieffer and J. Brooks (Springer New York, 2007) pp. 495–526.
- [18] A. Taheridehkordi, S. H. Curnoe, and J. P. F. LeBlanc, *Phys. Rev. B* **99**, 035120 (2019).
- [19] H. Elazab, B. D. E. McNiven, and J. P. F. LeBlanc, arXiv , 2201.09868 (2022).
- [20] A. Taheridehkordi, S. H. Curnoe, and J. P. F. LeBlanc, *Phys. Rev. B* **102**, 045115 (2020).
- [21] A. Taheridehkordi, S. H. Curnoe, and J. P. F. LeBlanc, *Phys. Rev. B* **101**, 125109 (2020).
- [22] B. D. E. McNiven, H. Terletska, G. T. Andrews, and J. P. F. LeBlanc, arXiv , 2203.09657 (2022).
- [23] B. D. E. McNiven, G. T. Andrews, and J. P. F. LeBlanc, *Phys. Rev. B* **104**, 125114 (2021).
- [24] T. A. Maier and D. J. Scalapino, *Phys. Rev. B* **84**, 180513 (2011).
- [25] G. Rohringer, A. Valli, and A. Toschi, *Phys. Rev. B* **86**, 125114 (2012), arXiv:1202.2796 [cond-mat.str-el].
- [26] T. M. Rice, K.-Y. Yang, and F. C. Zhang, *Reports on Progress in Physics* **75**, 016502 (2011).
- [27] J. P. F. LeBlanc, J. P. Carbotte, and E. J. Nicol, *Phys. Rev. B* **81**, 064504 (2010).